CMI

www.nature.com/cmi

ARTICLE

The OX40-TRAF6 axis promotes CTLA-4 degradation to augment antitumor CD8$^+$ T-cell immunity

Jizhang Yu[1,2,3,4,6], Jikai Cui[1,2,3,6], Xi Zhang[1,2,3,6], Heng Xu[1,2,3], Zhang Chen[1,2,3], Yuan Li[1,2,3], Yuqing Niu[1,2,3], Song Wang[1,2,3], Shuan Ran[1,2,3], Yanqiang Zou[1,2,3], Weicong Ye[1,2,3], Dan Zhang[3,5], Cheng Zhou[1,2], Jiahong Xia[1,2,3,4]✉ and Jie Wu[1,2,3,4]✉

Immune checkpoint blockade (ICB), including anti-cytotoxic T-lymphocyte associated protein 4 (CTLA-4), benefits only a limited number of patients with cancer. Understanding the in-depth regulatory mechanism of CTLA-4 protein stability and its functional significance may help identify ICB resistance mechanisms and assist in the development of novel immunotherapeutic modalities to improve ICB efficacy. Here, we identified that TNF receptor-associated factor 6 (TRAF6) mediates Lys63-linked ubiquitination and subsequent lysosomal degradation of CTLA-4. Moreover, by using TRAF6-deficient mice and retroviral overexpression experiments, we demonstrated that TRAF6 promotes CTLA-4 degradation in a T-cell-intrinsic manner, which is dependent on the RING domain of TRAF6. This intrinsic regulatory mechanism contributes to CD8$^+$ T-cell-mediated antitumor immunity in vivo. Additionally, by using an OX40 agonist, we demonstrated that the OX40-TRAF6 axis is responsible for CTLA-4 degradation, thereby controlling antitumor immunity in both tumor-bearing mice and patients with cancer. Overall, our findings demonstrate that the OX40-TRAF6 axis promotes CTLA-4 degradation and is a potential therapeutic target for the improvement of T-cell-based immunotherapies.

Keywords: Antitumor immunity; CD8$^+$ T cell; T-cell-based immunotherapy; TRAF6; CTLA-4

Cellular & Molecular Immunology (2023) 20:1445–1456; https://doi.org/10.1038/s41423-023-01093-y

INTRODUCTION

Cytotoxic T-lymphocyte associated protein 4 (CTLA-4), an important immune checkpoint receptor prominently expressed on activated T cells, contributes to immune homeostasis and tumor immune evasion [1–3]. The blocking antibody for CTLA-4, ipilimumab, had received approval from the US Food and Drug Administration (FDA) in 2011 for the treatment of malignant tumors, which makes it the first immune checkpoint receptor to be clinically targeted [4–6]. Although ipilimumab has shown durable responses in patients with advanced melanoma [7], the overall response rate in ipilimumab trials was less than 30% [8, 9]. Due to its superior benefit, anti-CTLA-4 antibodies are widely used in combination with other immune checkpoint blockade (ICB) therapies in the clinic [10]. Therefore, understanding the in-depth regulatory mechanism of CTLA-4 protein stability and its functional significance may help to identify ICB resistance mechanisms and assist in the development of novel immunotherapeutic modalities to improve ICB efficacy. Moreover, the expression of CTLA-4 on alloreactive T cells is essential for tolerance induction in transplantation [11, 12]. CTLA-4-Ig, an analog of CTLA-4 with equivalent functions, inhibits T-cell activation and is highly effective in prolonging the survival of humans and mice with transplantation and autoimmune disease [13–15]. As an important immune regulator, CTLA-4 expression is regulated through both transcriptional and post-transcriptional mechanisms in T cells. At the transcriptional level, *CTLA4* is regulated by several transcription factors, such as FOXO1 [16], NFAT1 [17], and FOXP3 [18]. Moreover, dysfunction of lipopolysaccharide-responsive and beige-like anchor (LRBA) increases the autophagy-lysosomal degradation of CTLA-4, resulting in CTLA-4 deficiency and T-cell dysregulation [19]. Although the essential roles of CTLA-4 in cancer progression are thoroughly understood, the regulatory mechanism of CTLA-4 protein stability and its functional significance remain elusive.

TNF receptor-associated factor 6 (TRAF6), a RING finger-domain E3 ubiquitin ligase, has a dual role in the regulation of immune system development, function, and pathogenesis, functioning as both a positive and negative regulator of immune cell signaling [20–22]. TNF receptor superfamily member 4 (TNFRSF4/OX40/CD134) is a T-cell costimulatory molecule that induces TRAF6 activation [23] and favors the induction of T helper 9 (Th9) cells [24]. Meanwhile, numerous studies have demonstrated that TRAF6 plays an essential role in innate immune cell activation and inflammatory responses by enhancing the transcriptional activation of nuclear factor-κB (NF-κB) signaling [25, 26]. However, King et al. demonstrated that the T-cell-specific deletion of

[1]Department of Cardiovascular Surgery, Union Hospital, Tongji Medical College, Huazhong University of Science and Technology, Wuhan, China. [2]Key Laboratory of Organ Transplantation, Ministry of Education, NHC Key Laboratory of Organ Transplantation, Key Laboratory of Organ Transplantation, Chinese Academy of Medical Sciences, Wuhan, China. [3]Center for Translational Medicine, Union Hospital, Tongji Medical College, Huazhong University of Science and Technology, Wuhan, China. [4]Institute of Translational Medicine, Tongji Medical College, Huazhong University of Science and Technology, Wuhan, China. [5]Cancer Center, Union Hospital, Tongji Medical College, Huazhong University of Science and Technology, Wuhan, China. [6]These authors contributed equally: Jizhang Yu, Jikai Cui, Xi Zhang. ✉email: jiahong.xia@mail.hust.edu.cn; wujie426@hust.edu.cn

Received: 19 March 2023 Accepted: 8 October 2023
Published online: 7 November 2023

TRAF6 surprisingly led to splenomegaly and lymphadenopathy in mice over 12 weeks old [27], suggesting that it is also a negative regulator of T cells. In addition, recent studies have indicated that TRAF6 plays a vital role in the differentiation of interleukin (IL)-9-producing $CD4^+$ T cells (Th9 cells), a distinct T helper cell subset that contributes to airway inflammation and antitumor immunity [28, 29]. However, it is poorly understood whether (and how) the OX40-TRAF6 axis affects the antitumor activity of $CD8^+$ T cells.

This study demonstrated that TRAF6 mediates the ubiquitination and degradation of CTLA-4 in a T-cell-intrinsic manner, and is essential for the antitumor activity of $CD8^+$ T cells. Furthermore, both TRAF6 expression and CTLA-4 degradation are regulated by the OX40-TNF superfamily member 4 (TNFSF4/OX40L) pathway. The antitumor efficacy of the OX40 agonist, which is dependent on TRAF6 expression, coordinates with programmed cell death 1 (PDCD1/PD-1) but not CTLA-4 blockade. Therefore, the OX40-TRAF6-CTLA-4 axis is a potential therapeutic target for improving T-cell-based immunotherapies.

MATERIALS AND METHODS

Mice

C57BL/6 J (B6, N000013), BALB/c (B/c, N000020), B6-CD45.1 (B6/JGpt-*Ptprc*$^{em1Cin\ (p.\ K302E)}$/Gpt, T054816), and *Rag1*$^{-/-}$ mice (B6/JGpt-Rag1^{em1Cd}/Gpt, T004753) were obtained at least one week prior to the experiment from GemPharmatech (Nanjing, China). *Traf6*$^{C70A/WT}$ (B6/JGpt-*Traf6*$^{em1Cin(C70A)}$/Gpt, T055143) mice were generated and purchased from GemPharmatech (Nanjing, China). *CD4-cre* (B6. Cg-Tg[*Cd4-cre*]1Cwi/BfluJ, #022071) and OT-I (C57BL/6-Tg[TcraTcrb]1100Mjb/J, #003831) mice were ordered from Jackson Laboratory, while the *Traf6*$^{fl/fl}$ (C57BL/6 N-A^{tm1Brd}*Traf6*$^{tm2a(EUCOMM)Wtsi}$/WtsiOulu, #08446, the European Mouse Mutant Archive) mice were gifted by Dr. Peng Zhang (Wuhan University, China). The breeding and husbandry of the mice were completed in a specific pathogen-free (SPF) environment (23 ± 3 °C, 12-h light/dark cycle) provided by Tongji Medical College, Huazhong University of Science and Technology. All animal procedures and experimental operations conformed to the Code for Care and Use of Experimental Animals of the Laboratory Animal Center set by Tongji Medical College. The Institutional Ethics Committee of Tongji Medical College approved all animal experiments and procedure designs (XWK-YZMY-085).

Tumor models

All mice were fed and cared for in the SPF facility. Male mice aged 7–11 weeks old were used for the experiments, with sex-matched littermates used as controls. Tumor cells (diluted in phosphate-buffered saline [PBS]) were subcutaneously injected into the right groin of each mouse on day 0. Tumor sizes were measured and recorded with calipers every two to four days. Mice were sacrificed when tumors exceeded 2000 mm^3 or when they became moribund. Mice were sacrificed via CO_2 asphyxiation to obtain the tumors. For details, please see Supplementary Materials.

The SPARK system

The SPARK system was used according to the previous study [30]. The SPARK reporting systems were gifted by Dr. Xiaokun Shu. The cDNA sequences of CTLA-4 and TRAF6 were cloned into SPARK vectors. SPARK vectors containing only CTLA-4 or TRAF6 were used as controls. HEK293T cells were generated and cultured in vitro. Transfection was performed using the Neofect transfection reagent (Neofect Biotech) when cells were cultured to 50% confluence in confocal dishes. Cultures were carried out in accordance with the manufacturer's instructions. Cells were imaged 24 h post-transfection using confocal microscopy (Nikon A1Si). The number of puncta was assessed for summary statistics.

EAE model

The EAE modeling method was based on the previous research [31]. For details, please see the Supplementary Materials.

FCM analysis

Single-cell suspensions were prepared, stained, and evaluated according to the previous research [32]. For details, please see the Supplementary Materials.

Statistical analysis

The results were analyzed using GraphPad Prism 9.2.0 (https://www.graphpad-prism.cn/) and presented as the mean ± SD or mean ± s.e.m. To compare two groups, *P* values were calculated by using a two-tailed unpaired Student's *t*-test for Gaussian distributed data when the variances were similar and Welch's *t*-test when the variances were different. The Wilcox test was used for large samples ($n > 10$) comparing two groups. For comparisons of three or more groups, *P* values were calculated by using one-way or two-way analysis of variance (ANOVA) for normally distributed data, followed by Dunnett's or Sidak's multiple comparisons test. The log-rank test was used for Kaplan–Meier survival analysis. Each experiment was repeated for three times independently with similar results. The number of animals and methods of the statistical tests used for each experiment are indicated in the corresponding figure legends.

RESULTS

TRAF6 is an E3 ubiquitin ligase that mediates K63-linked polyubiquitination of CTLA-4

The dynamic expression of CTLA-4 was examined in activated T cells at different time points by using the flow cytometry (FCM) assay. Upon in vitro activation, the protein level of CTLA-4 in $CD4^+$ and $CD8^+$ T cells peaked at approximately 48 h and declined at 72 h (Fig. 1A, B). Similarly, we found that *Ctla4* mRNA expression was downregulated at 72 h after peaking at approximately 48 h (Fig. 1C). Our previous study revealed that CTLA-4 degradation is inhibited by chloroquine administration and promoted by MG132 treatment [33]. In addition, other studies have suggested that CTLA-4 is degraded via the autophagic-lysosomal pathway [19, 34]. Given that ubiquitination is the most common modification prior to protein degradation, the ubiquitination of CTLA-4 was found in activated mouse splenic T cells (Fig. 1D). The ubiquitination of CTLA-4 was also detected at 24, 48, and 72 h post-activation in mouse $CD8^+$ T cells (Fig. 1E). To identify the potential E3 ubiquitin ligase that interacts with CTLA-4, coimmunoprecipitation (co-IP) and mass spectrometry (MS) experiments were performed with activated murine T cells, identifying TRAF6, a molecule with E3 enzyme activity (Fig. 1F). Multispecies alignments of CTLA-4 proteins determined that the conserved protein domains of CTLA-4 contained the TRAF6-binding motif [35] (Fig. 1G), signifying that TRAF6 is a viable candidate for further investigation.

An endogenous co-IP assay was used to verify the binding of CTLA-4 to TRAF6. CTLA-4 was found to bind to TRAF6 in activated mouse $CD8^+$ T cells (Fig. 1H). HEK293T cells were transfected with MYC–CTLA-4 and FLAG–TRAF6, and the interaction between TRAF6 and CTLA-4 was confirmed using a reciprocal co-IP assay (Fig. 1I). The separation of phases-based activity reporter of kinase (SPARK) system was used to visualize the formation of the CTLA-4–TRAF6 complex (Fig. S1A). In brief, during the formation of the CTLA-4-TRAF6 complex, CTLA-4-enhanced green fluorescence protein (EGFP)-homo-oligomeric tag 3 (HOTag3) hexamers cross-link with TRAF6-homo-oligomeric tag 6 (HOTag6) tetramers to induce EGFP phase separation [30]. Live-cell fluorescence imaging demonstrated that co-transfection of HEK293T cells with CTLA-4-EGFP-HOTag3 and TRAF6-HOTag6 resulted in the formation of numerous green fluorescent puncta, which were not present in the control groups (Fig. 1J). We visualized the CTLA-4/TRAF6 complex specifically based on a proximity ligation assay (PLA, Fig. S1B). In addition, overexpression of TRAF6 significantly increased the ubiquitin modification of CTLA-4 in a dose-dependent manner (Fig. 1K). Furthermore, a mutation in the TRAF6 RING domain (C70A), which inhibits the E3 ligase activity of TRAF6, attenuated the ability of TRAF6 to induce ubiquitin modification of CTLA-4 [36] (Fig. 1L).

K48- and K63-linked polyubiquitination are the most abundant and functionally well-characterized linkage types prior to protein degradation [37]. To determine the main linkage type in

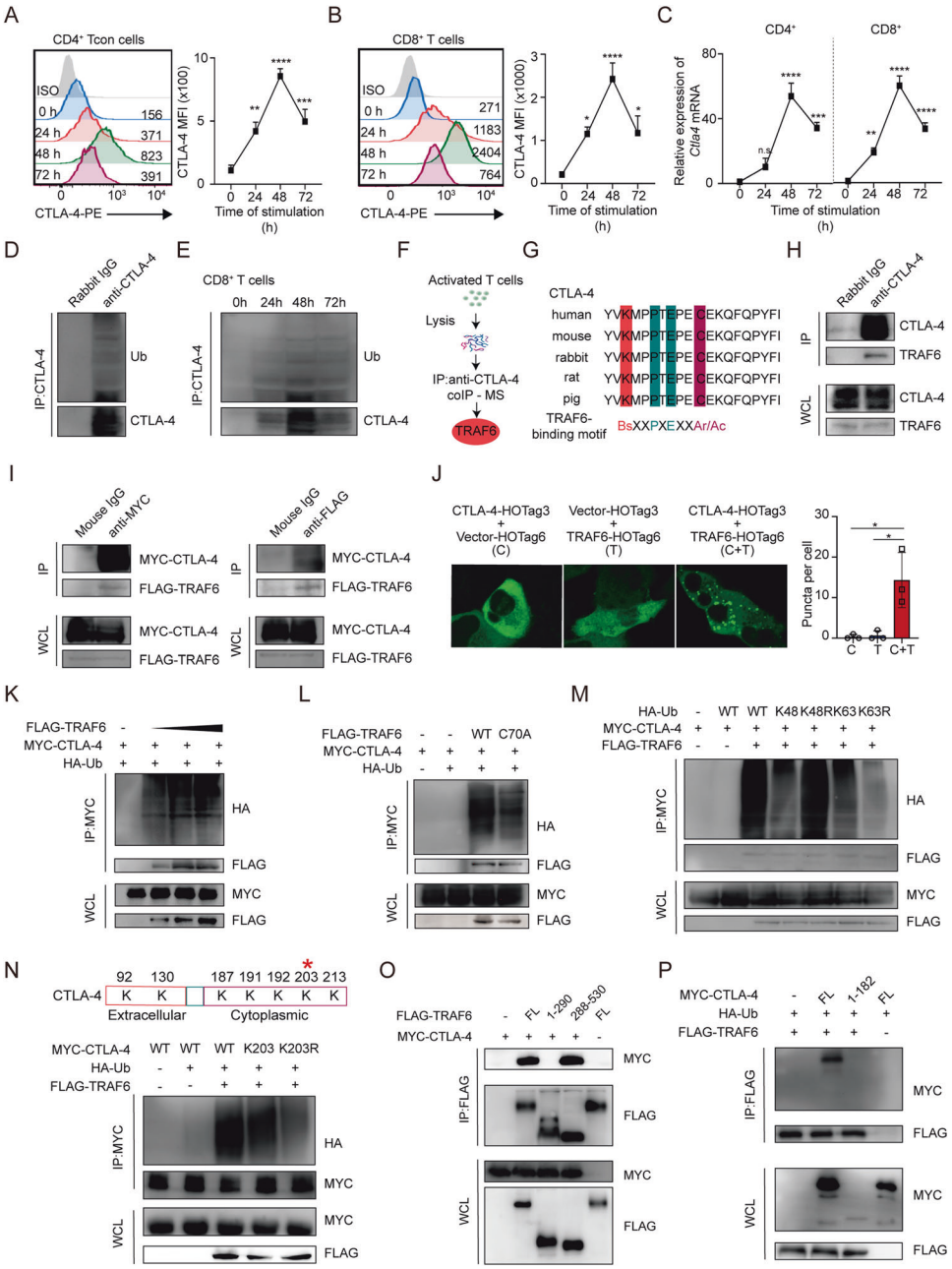

Fig. 1 TRAF6 is an E3 ubiquitin ligase that mediates K63-linked polyubiquitination of CTLA-4. Murine $CD4^+$ Tcon cells ($CD4^+CD25^-$ T cells) and $CD8^+$ T cells were isolated, activated by using the Dynabeads Mouse T-Activator CD3/CD28, and collected for the analysis at different time points. **A** Representative histograms and line graphs of the protein expression (MFI) and the proportion of positive cells of CTLA-4 in $CD4^+$ Tcon cells ($CD4^+CD25^-$ T cells) at 0, 24, 48, and 72 h post-activation. One-way ANOVA test. **B** Representative histograms and line graphs of the protein expression (MFI) and the proportion of positive cells of CTLA-4 in $CD8^+$ T cells at 0, 24, 48, and 72 h post-activation. One-way ANOVA test. **C** Line graphs of *Ctla4* mRNA expression in $CD4^+$ and $CD8^+$ T cells at 0, 24, 48, and 72 h post-activation. One-way ANOVA test. **D** CTLA-4 polyubiquitination detection in activated primary mouse T cells. **E** CTLA-4 polyubiquitination detection in $CD8^+$ T cells at 0, 24, 48, and 72 h post-activation. **F** The procedure used to identify the E3 ubiquitin ligases interacting with CTLA-4 via co-IP/MS analysis. **G** The multispecies protein alignments for CTLA-4 by using the TRAF6-binding motif. **H** Co-IP of CTLA-4 and TRAF6 in activated primary mouse T cells. **I** Co-IP of CTLA-4 and TRAF6 in HEK293T cells transfected with the indicated plasmids. **J** Fluorescence imaging of HEK293T cells expressing CTLA-4-HOTag3 and Vector-HOTag6, Vector-HOTag3 and Traf6-HOTag6, or CTLA-4-HOTag3 and TRAF6-HOTag6. Two-way ANOVA test. (C, CTLA-4-HOTag3 and Vector-HOTag6; T, Vector-HOTag3 and TRAF6-HOTag6; C + T, CTLA-4-HOTag3 and TRAF6-HOTag6). **K** Western blots show the levels of CTLA-4 polyubiquitination in HEK293T cells transfected with MYC–CTLA-4, HA–ubiquitin (Ub), and different amounts of FLAG–TRAF6 plasmids. **L** Western blots show the levels of CTLA-4 polyubiquitination HEK293T cells transfected with MYC–CTLA-4, HA–Ub, and the indicated TRAF6 WT or mutant plasmids. **M** Measurement of CTLA-4 ubiquitination type in HEK293T cells. **N** IP analysis measured the CTLA-4 ubiquitination site in HEK293T cells transfected with the indicated plasmids. **O** The interaction of CTLA-4 with the indicated truncations of TRAF6. **P** The interaction of TRAF6 with the indicated truncation of CTLA-4. Please also see Fig. S1

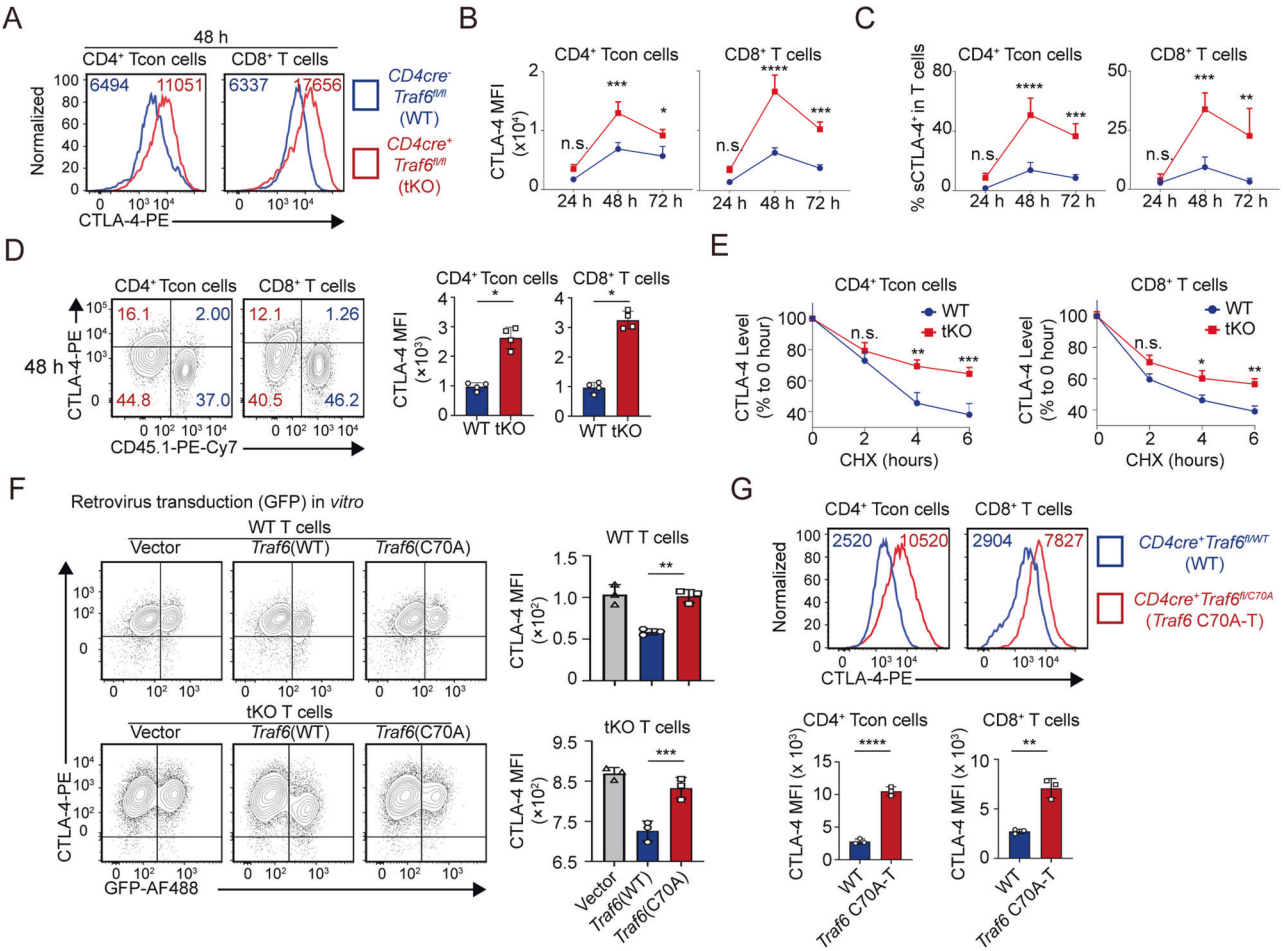

Fig. 2 The loss of TRAF6 E3 ligase activity attenuates CTLA-4 degradation in a T-cell-intrinsic manner. **A** Representative histograms of CTLA-4 expression in $CD4^+$ Tcon cells ($CD4^+CD25^-$ T cells) and $CD8^+$ T cells ($CD8^+$ T cells) from *Traf6*-tKO mice and WT mice at 48 h post-activation. **B** Line graphs of CTLA-4 expression (MFI) of $CTLA\text{-}4^+$ cells in $CD4^+$ Tcon ($CD4^+CD25^-$T cells) and $CD8^+$ T cells ($CD8^+$ T cells) of *Traf6*-tKO mice and WT mice at 24 h, 48 h and 72 h post-activation. Two-way ANOVA test. **C** Line graphs of the percentage of $CTLA\text{-}4^+$ cells in $CD4^+$ Tcon ($CD4^+CD25^-$ T cells) and $CD8^+$ T cells ($CD4^+CD25^-$ T cells) of *Traf6*-tKO mice and WT mice at 24 h, 48 h, and 72 h post-activation. Two-way ANOVA test. **D** Representative contour plots and bar plots of CTLA-4 expression at 48 h post-activation. ($n = 4$). Two-tailed unpaired Student's *t*-test. **E** Line graphs of CTLA-4 levels in activated tKO and WT T cells at 0, 2, 4, and 8 h post-CHX treatment. The expression of CTLA-4 was measured by FCM. Two-way ANOVA test. **F** Representative contour and bar plots of CTLA-4 expression in $CD8^+$ T cells after transfection with *Traf6*(WT) or *Traf6*(C70A) vectors. One-way ANOVA test and two-tailed unpaired Student's *t*-test were performed. **G** Representative histograms of CTLA-4 expression in $CD4^+$ Tcon and $CD8^+$ T cells from *Traf6* C70A mice and WT mice 48 h post-activation in vitro. Histograms show the quantification of CTLA-4 expression ($n = 3$). Two-tailed unpaired Student's *t*-test. Error bars represent SD, and ns indicates non-significant results; $^*P < 0.05$, $^{**}P < 0.01$, $^{***}P < 0.001$, and $^{****}P < 0.0001$. Please also see Figs. S2 and S3

polyubiquitinated CTLA-4, plasmids were constructed for ubiquitin mutants that permitted the formation of K48- or K63-linked chains individually (K48 or K63) or prevented their formation (K48R or K63R). The expression of K63R impaired the ubiquitination of CTLA-4, whereas the expression of K48R only had a minor impact (Fig. 1M). In silico analysis was conducted to predict the putative ubiquitination sites of CTLA-4 with two site-prediction software programs: SUMOplot and UbPred (Fig. S1C). To validate the prediction, CTLA-4 plasmids were constructed with K-to-R mutations to prevent TRAF6 modification. As expected, the mutation at position 203 of the CTLA-4 protein prominently prevented ubiquitination by TRAF6 (Fig. 1N). To further illuminate the in-depth molecular events occurring in the interactions between CTLA-4 and TRAF6, truncated TRAF6 and CTLA-4 proteins were designed and created (Fig. S1D). The TRAF-C domain (288 to 530 aa) and CTLA-4 cytoplasmic domain (183 to 223 aa) were essential for TRAF6 and CTLA-4 interaction (Fig. 1O, P). Therefore, TRAF6 is an E3 ubiquitin ligase that mediates the K63-linked polyubiquitination of CTLA-4.

The loss of TRAF6 E3 ligase activity attenuates CTLA-4 degradation in a T-cell-intrinsic manner

To further explore the effect of TRAF6 on CTLA-4 expression and cell function in T cells, *Traf6* T-cell-conditional knockout (*Traf6*$^{fl/fl}$*CD4-cre*$^+$, *Traf6* tKO) mice were generated by crossbreeding *Traf6*$^{fl/fl}$ and *CD4-cre*$^+$ mice. *Traf6*-tKO T cells were isolated from *Traf6*-tKO mice using age-matched littermate *Traf6*$^{fl/fl}$*CD4-cre*$^-$ (WT) mice as controls. To understand the role of TRAF6 in the expression of CTLA-4 in activated T cells, *Traf6* tKO and WT T cells were isolated and stimulated in vitro. Then, CTLA-4 expression was analyzed by FCM 24, 48, and 72 h post-stimulation in vitro. CTLA-4 expression in *Traf6*-tKO T cells was significantly increased in both $CD4^+CD25^-$ T cells (conventional T cells, Tcon) and $CD8^+$ T cells at each time point compared with WT T cells (Fig. 2A–C and Fig. S2A) [38]. To examine whether the effect of TRAF6 on CTLA-4 expression in T cells was intrinsic, $CD45.1^+$ WT T cells and $CD45.2^+$ *Traf6*-tKO T cells were co-cultured and stimulated for 48 h. The loss of TRAF6 in T cells resulted in a marked increase in the protein level of CTLA-4 (Fig. 2D). However, the expression of *Ctla4* mRNA did not differ between the two groups (Fig. S2B).

To test the hypothesis that TRAF6 ablation attenuated CTLA-4 degradation, activated $CD4^+$ Tcon and $CD8^+$ T cells were treated with 100 μg/mL cycloheximide (CHX) to block nascent protein synthesis. The degradation of CTLA-4 was significantly slower in *Traf6*-tKO T cells compared with WT T cells (Fig. 2E). To further verify whether the regulatory activity of TRAF6 on CTLA-4 degradation is dependent on its E3 ligase activity, activated $CD8^+$ T cells from WT or *Traf6*-tKO mice were overexpressed with TRAF6, TRAF6 with C70A mutation, or GFP (control) by retroviral infection. Overexpressing TRAF6 significantly decreased CTLA-4 protein levels in both WT and *Traf6*-tKO T cells. However, this effect was not observed in the overexpression of TRAF6 with the C70A mutation (Fig. 2F). To further verify the effect of TRAF6 E3 ligase activity on CTLA-4 expression in vivo, CRISPR–Cas9 editing was used to introduce a loss-of-E3-function mutation in the *Traf6* gene in murine embryonic stem cells, yielding *Traf6* C70A heterozygous mice (Fig. S3A). Similar to *Traf6*-knockout mice [39], the *Traf6* C70A mutation was a homozygous lethal mutation (Fig. S3B).

Traf6 T-cell-conditional mutation ($Traf6^{fl/C70A}CD4\text{-}cre^+$, *Traf6* C70A-T) mice were generated by crossing $Traf6^{fl/fl}CD4\text{-}cre^+$ mice with heterozygous $Traf6^{C70A/WT}$ mice (Fig. S4B). The expression of CTLA-4 in activated *Traf6* C70A-T and $Traf6^{fl/WT}CD4\text{-}cre^+$ (WT) T cells was analyzed via FCM at 48 h. CTLA-4 expression in *Traf6* C70A-T T cells was significantly increased in both $CD4^+$ Tcon and $CD8^+$ T cells compared with controls (Fig. 2G). Overall, these results demonstrated that TRAF6 regulates the degradation and expression of CTLA-4 in a T-cell-intrinsic manner that is dependent on its ubiquitin activity.

Ablation of TRAF6 impairs antitumor $CD8^+$ T-cell immunity

Considering that T-cell-specific TRAF6-deficient mice spontaneously develop splenomegaly and lymphadenopathy [27], an adoptive transfer melanoma model was established to assess the effect of TRAF6 deficiency on the antitumor immunity of $CD8^+$ T cells. $Traf6^{fl/fl}CD4\text{-}cre^-$ (WT) or $Traf6^{fl/fl}CD4\text{-}cre^+$ (*Traf6* tKO) OT-I cells were adoptively transferred into B16-OVA-bearing WT mice (Fig. 3A). B16-OVA melanoma progression was accelerated in mice receiving TRAF6-deficient OT-I cells compared with WT OT-I cells (Fig. 3B, C). To further investigate the impact of TRAF6 ablation on the antitumor activity of T cells, $CD45.1^+CD8^+$ $Traf6^{fl/fl}CD4\text{-}cre^-$(WT) T cells and $CD45.2^+CD8^+$ $Traf6^{fl/fl}CD4\text{-}cre^+$ (*Traf6*-tKO) T cells were adoptively transferred at a 1:1 mixture into B16 melanoma-bearing $Rag1^{-/-}$ mice (Fig. 3D and Fig. S4A). FCM analysis of tumor-infiltrating lymphocytes (TILs) demonstrated a lower proportion of *Traf6*-tKO $CD8^+$ T cells compared with WT controls (Fig. 3E and Fig. S4B), suggesting that ablating TRAF6 impairs the antitumor activity of $CD8^+$ T cells.

To further assess the phenotypes of *Traf6*-tKO TILs, $CD8^+$ TILs were sorted using fluorescence-activated cell sorting (FACS), followed by transcriptome sequencing. Compared with WT TILs, a total of 239 genes were upregulated and 113 were downregulated in *Traf6*-tKO TILs (Fig. 3F). Among these, effector transcription factors (*Tbx21*, *Irf4*) [40], cytotoxic genes (*Gzmb*, *Prf1*), and receptors and adhesion molecules (*Cd38* and *E2f1*) were downregulated, whereas effector T-cell differentiation regulators (*Tcf7*) [41] and inhibitory cytokines (*Il10*) were upregulated (Fig. 3G). Pathway enrichment analysis determined that differentially expressed genes (DEGs) between *Traf6* tKO and WT TILs were involved in the positive regulation of leukocyte activation, leukocyte proliferation, T-cell-mediated immunity, immune effector processes, T-cell differentiation, and T-cell-mediated cytotoxicity (Fig. 3H). Specifically, gene-set enrichment analysis (GSEA) of DEGs demonstrated enrichment of leukocyte-mediated cytotoxicity, leukocyte proliferation, cell killing, leukocyte-mediated immunity, and T-cell differentiation (Fig. 3I and Fig. S4C).

An FCM assay was performed to assess the molecules related to the aforementioned pathways. We observed increases in expression of CTLA-4 and TCF-1^+ $CD8^+$ T cells in *Traf6*-tKO TILs, and a reduction in expression of $Ki67^+$ and $GZMB^+$ $CD8^+$ T cells in *Traf6*-tKO TILs (Fig. 3J). This suggests that TRAF6 deficiency impaired the proliferation and cytotoxic killing ability and promoted CTLA-4 expression in $CD8^+$ TILs in B16 subcutaneous tumor models. Overall, these results indicate that TRAF6 ablation impairs the antitumor activity of $CD8^+$ T cells.

Given that TRAF6 is an important regulator of T cells [29, 42], *Traf6*-tKO mice were tested in heart transplantation models and experimental allergic encephalomyelitis (EAE) models. The ablation of TRAF6 in T cells attenuated acute cardiac allograft rejection (Fig. S2E). Likewise, *Traf6*-tKO mice were almost completely resistant to EAE induction compared with control mice, indicating that TRAF6 plays an important role in regulating T-cell encephalitogenicity (Fig. S2F). These experiments were repeated in *Traf6* C70A-T mice. This revealed that the RING domain mutant TRAF6 C70A in T cells also attenuated acute cardiac allograft rejection (Fig. S3C) and EAE induction compared with control mice (Fig. S3D).

Elevated TRAF6 augments antitumor $CD8^+$ T-cell immunity

Given that TRAF6 deficiency in $CD8^+$ T cells impaired their antitumor ability, the question was raised as to whether TRAF6 overexpression augments the antitumor response of $CD8^+$ T cells. First, OT-I T cells were retrovirally transduced with vectors encoding TRAF6 or GFP (control). Quantitative tandem mass tag (TMT)-based proteomic analysis was used to assess cellular protein expression (Fig. 4A and Fig. S5A). A volcano plot revealed that 103 proteins were significantly upregulated and 58 proteins were significantly downregulated in *Traf6*-OE OT-I T cells (Fig. 4B). The pathway enrichment analysis of the differentially expressed proteins (DEPs) involved activation pathways (positive regulation of leukocyte activation), proliferation pathways (regulation of leukocyte proliferation), defense response pathways (leukocyte cell-cell adhesion, immune response-related leukocyte activation, and positive regulation of leukocyte migration), and cytotoxicity (regulation of immune effector process; Fig. 4C). The GSEA of DEPs also demonstrated enrichment of leukocyte-mediated cytotoxicity and leukocyte proliferation (Fig. 4D and Fig. S5B). CTLA-4 was consistently downregulated. However, cytotoxic molecules (GZMB and perforin) and a T-cell receptor (TCR)-induced transcription factor (IRF4) were upregulated in *Traf6*-OE OT-I T cells (Fig. 4E).

To further verify whether TRAF6 overexpression promoted the antitumor response of $CD8^+$ T cells, we adoptively transferred *Traf6*-OE or empty vector (EV) $CD45.2^+$ OT-I cells into B16-OVA-bearing $CD45.1^+$ WT mice (Fig. 4F). Compared with EV OT-I cells, *Traf6*-OE OT-I cells exhibited better antitumor efficacy, as smaller tumors were observed in the *Traf6*-OE group (Fig. 4G, H). An increase in tumor-infiltrating OT-I cells in the *Traf6*-OE group was observed on post-cell transfer day 10 compared with the EV group (Fig. 4H, I). Furthermore, overexpression of *Traf6* significantly augmented the expression of Ki67, GZMB, perforin, and CD107a in tumor-infiltrating OT-I cells, which was associated with the proliferation and cytotoxic function of T cells (Fig. 4J–M). Moreover, *Traf6* overexpression decreased the expression of T-cell exhaustion transcription factor (TCF-1, Fig. 4N) and CTLA-4 (Fig. 4O). There was no significant difference in TOX expression between the two groups (Fig. S5E). Together, these results showed that elevated TRAF6 expression promotes the antitumor function of $CD8^+$ T cells.

The OX40-TRAF6 axis promotes CTLA-4 degradation and antitumor responses

Previous studies have reported that OX40 signaling drives TRAF6 expression in $CD4^+$ T cells and promotes Th9 cell differentiation [24, 43, 44]. However, the effect of OX40 signaling on TRAF6 expression and the antitumor function of $CD8^+$ T cells is unclear. Similar to previous observations in $CD4^+$ T cells, the anti-OX40 agonist antibody (OX86) promoted TRAF6 expression in activated $CD8^+$ T cells (Fig. 5A). CTLA-4 expression was determined at the

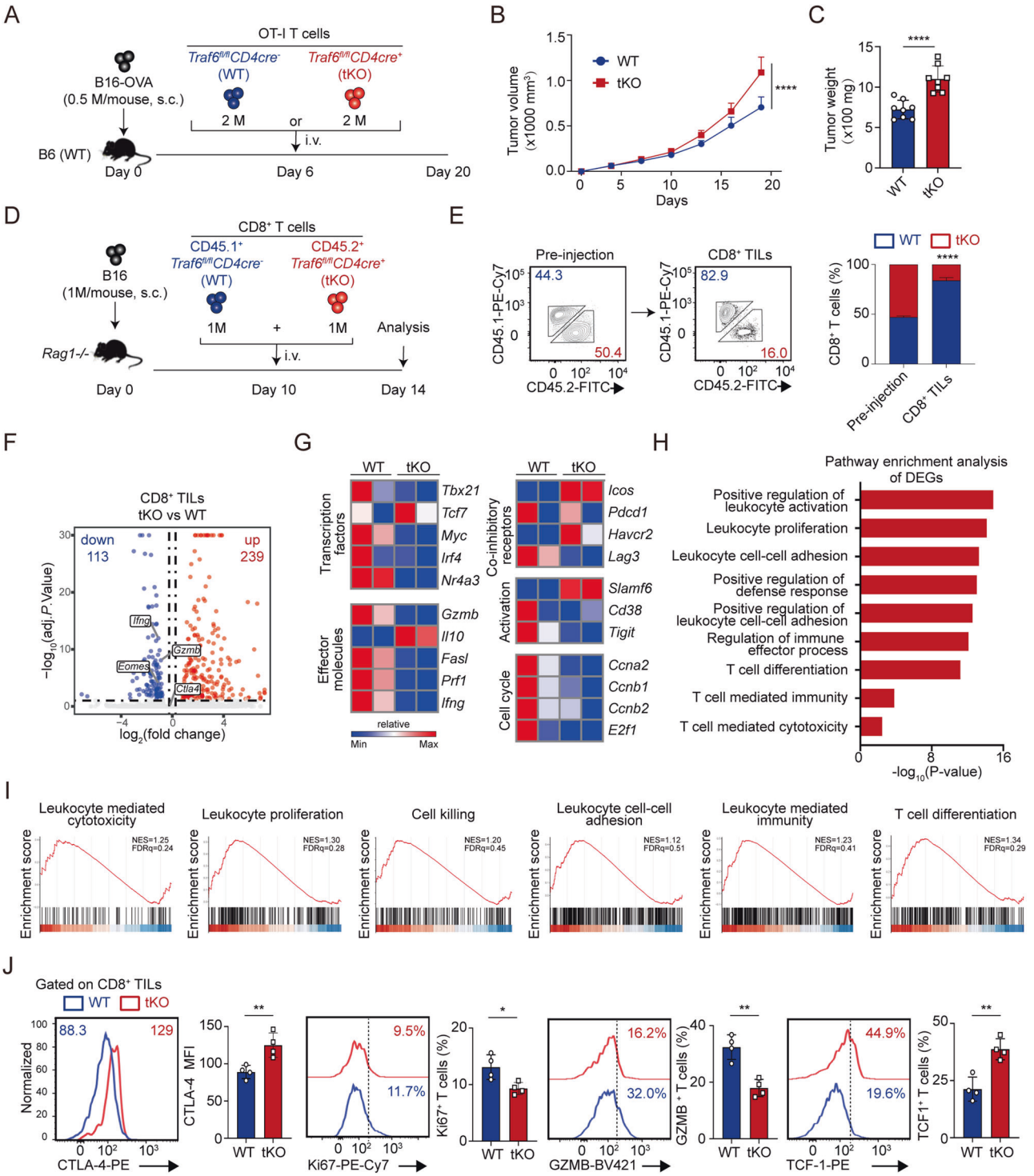

Fig. 3 Ablation of TRAF6 impairs the antitumor activity of CD8$^+$ T cells. **A** Schematic of the workflow of the animal experiments. **B** Growth curves of B16-OVA melanoma in B6 mice that underwent the adoptive transfer of WT or *Traf6*-tKO OT-I cells ($n = 10$). Two-way ANOVA test. **C** Bar plots show tumor weight of B16-OVA melanoma in B6 mice that underwent the adoptive transfer of WT or *Traf6*-tKO OT-I cells on day 20. Two-tailed unpaired Student's *t*-test was performed. **D** Schematic of the workflow of the animal experiments. **E** Representative histograms of the proportions of CD45.1$^+$CD8$^+$ TILs and CD45.2$^+$CD8$^+$ TILs before and after injection ($n = 4$). Two-tailed unpaired Student's t-test. (F to H) WT and *Traf6*-tKO CD8$^+$ TILs were sorted and collected for RNA-seq. **F** A volcano plot of the DEGs between *Traf6*-tKO CD8$^+$ T cells and WT CD8$^+$ T cells. **G** A heatmap of representative genes between *Traf6*-tKO CD8$^+$ T cells and WT CD8$^+$ T cells. **H** The pathway enrichment analysis of the identified DEGs. **I** A GSEA barcode plot of the representative signaling pathways in WT CD8$^+$ T cells versus *Traf6*-tKO CD8$^+$ T cells. NES (normalized enrichment score), FDRq (false discovery rate *q*-values). **J** Representative histograms and bar plots of CTLA-4 expression (MFI) in CD8$^+$ TILs and proportions of Ki67$^+$ cells, GZMB$^+$ cells, and TCF-1$^+$ cells in CD8$^+$ TILs on day 14 ($n = 4$). Two-tailed unpaired Student's *t*-test. Error bars represent SD. *$P < 0.05$, **$P < 0.01$, ***$P < 0.001$, and ****$P < 0.0001$. Please also see Fig. S4

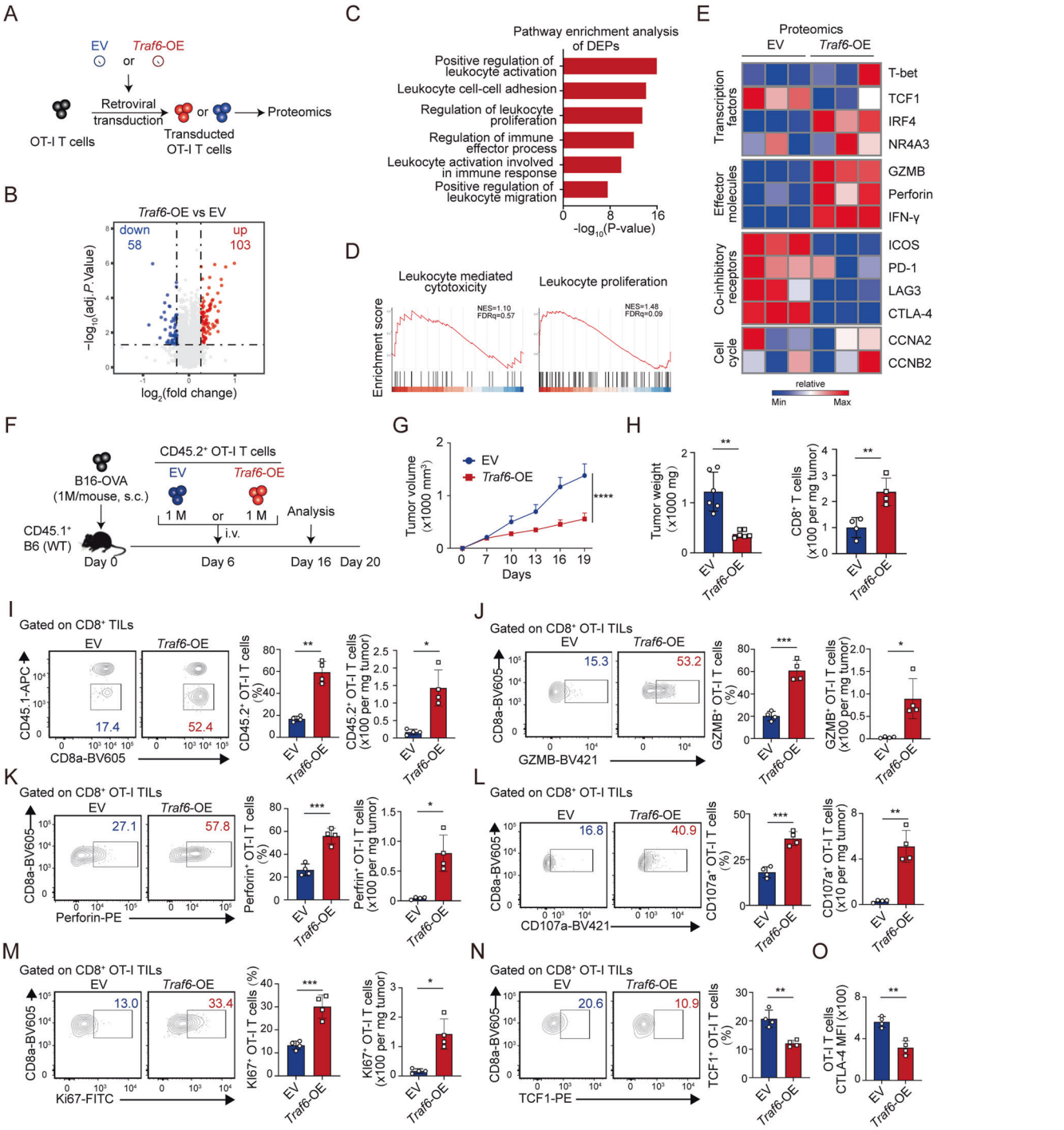

Fig. 4 Elevated TRAF6 promotes the antitumor function of CD8$^+$ T cells. **A** Schematic of the workflow of the proteomics study (**B**–**E**). **B** A volcano plot of the DEPs between EV OT-I cells and Traf6-OE OT-I cells. **C** The pathway enrichment analysis of the identified DEPs. **D** A GSEA barcode plot of *Traf6*-OE OT-I cells versus EV OT-I cells. **E** A heatmap of the representative proteins between *Traf6*-OE OT-I cells and EV OT-I cells. **F** Schematic of the workflow of the animal experiments. **G** Growth curves of B16-OVA melanoma in CD45.1$^+$ B6 mice that underwent the adoptive transfer of EV or *Traf6*-OE OT-I cells ($n = 6$). Two-way ANOVA test. **H** Bar plots demonstrating tumor weight and cell numbers of CD8$^+$ cells in B16-OVA melanoma tumor masses ($n = 4$, $n = 6$). Two-tailed unpaired Student's *t*-test and unpaired *t*-test with Welch's correction were performed. **I** Contour plots and bar plots of tumor-infiltrating OT-I cell proportions and numbers ($n = 4$). Unpaired *t*-test with Welch's correction. **J**–**N** Contour plots and bar plots of the percentage and numbers of GZMB$^+$ cells, Perforin$^+$ cells, Ki67$^+$ cells, CD107a$^+$ cells, and TCF-1$^+$ cells in OT-I TILs ($n = 12$). Two-tailed unpaired Student's *t*-test and unpaired *t*-test with Welch's correction were performed. **O** Bar plots of CTLA-4 expression (MFI) in tumor-infiltrating OT-I cells ($n = 4$). Two-tailed unpaired Student's *t*-test. In **H**–**O** the data represent means ± SD. And in G, the data represent means ± s.e.m. *$P < 0.05$, **$P < 0.01$, ***$P < 0.001$, ****$P < 0.0001$. Please also see Fig. S5

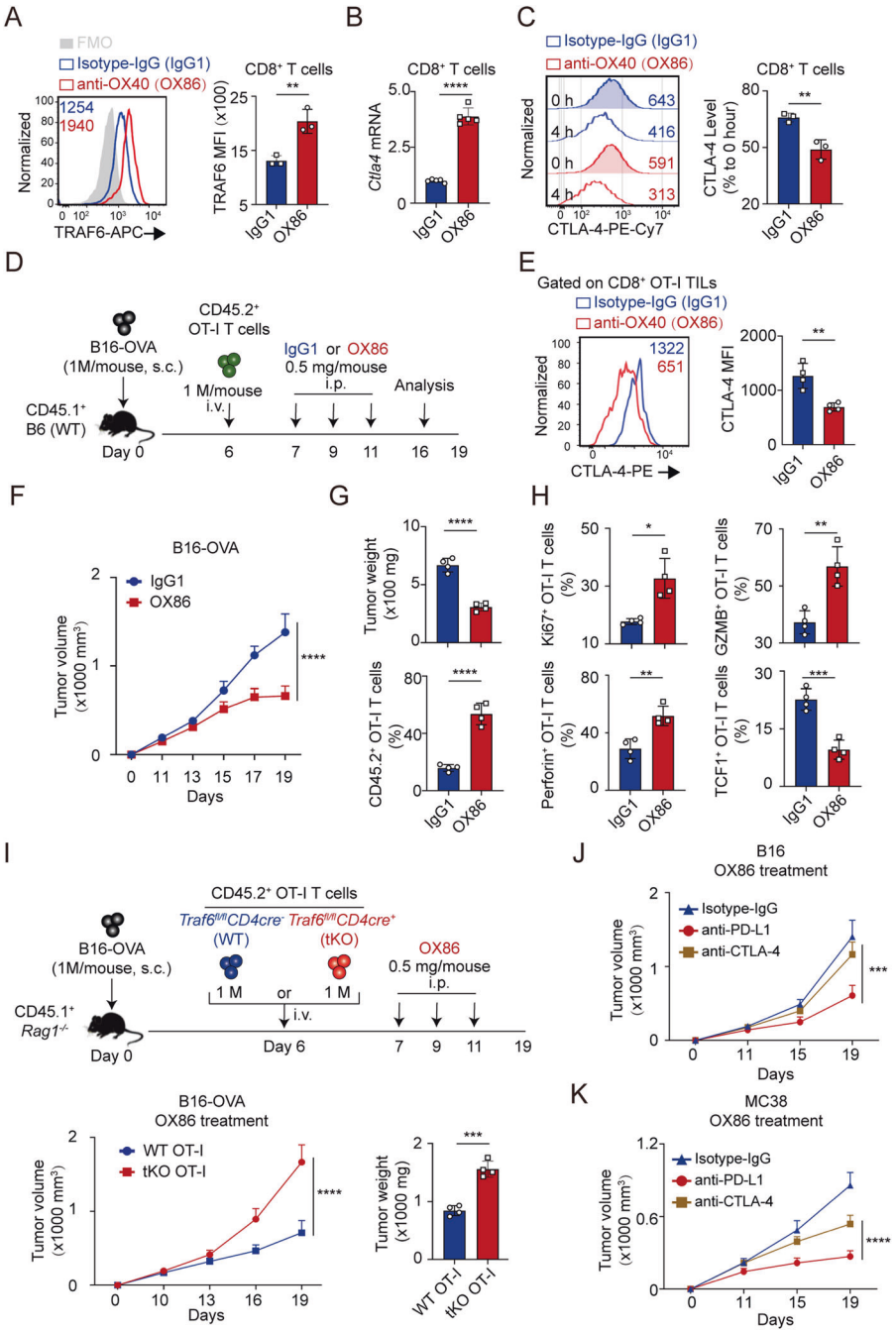

Fig. 5 The OX40-TRAF6 axis promotes CTLA-4 degradation and antitumor responses. **A** Representative histograms and bar plots of TRAF6 expression in activated T cells in the isotype-IgG1 and OX86 groups ($n = 3$). Two-tailed unpaired Student's *t*-test. **B** Bar plots of *Ctla4* mRNA expression in activated T cells in the isotype-IgG1 and OX86 groups ($n = 5$). Two-tailed unpaired Student's *t*-test. **C** Representative histograms and bar plots of CTLA-4 expression in $CD8^+$ T cells in the isotype-IgG1 or OX86 groups before CHX treatment and 4 h post-treatment ($n = 3$). Two-tailed unpaired Student's *t*-test. **D** Schematic of the workflow of the animal experiments. **E** Representative histograms and bar plots of CTLA-4 expression in OT-I TILs in the isotype-IgG1 and OX86 groups. Two-tailed unpaired Student's *t*-test was performed. **F** Growth curves of B16-OVA in $CD45.1^+$ B6 mice in the isotype-IgG1 and OX86 groups. ($n = 12$). Two-way ANOVA test. **G** Bar plots of tumor weight and the proportion of OT-I cells in $CD8^+$ TILs ($n = 6$). Two-tailed unpaired Student's *t*-test. **H** Bar plots of the percentages of $GZMB^+$ cells, $perforin^+$ cells, $Ki67^+$ cells, and $TCF\text{-}1^+$ cells in OT-I TILs ($n = 4$). Two-tailed unpaired Student's *t*-test and unpaired *t*-test with Welch's correction were performed. **I** Schematic of the workflow of the animal experiments. Growth curves of B16-OVA in $CD45.1^+$ $Rag1^{-/-}$ mice that underwent the adoptive transfer of WT or tKO OT-I cells and were treated with OX86 ($n = 8$, 10). Bar plots of the tumor weights on day 19 ($n = 4$). Two-tailed unpaired Student's *t*-test and two-way ANOVA followed by Bonferroni post-hoc test. **J**, **K** Growth curves of B16 and MC38 cells in B6 mice treated with OX86 plus isotype-IgG, anti-PD-L1 or anti-CTLA-4 antibody. ($n = 8$). Two-way ANOVA test. In **A**–**E**, **G**, **H**, **I** the data of bar plots represent means ± SD. And in **F**, **I**, **J**, and **K** the data of growth curves represent means ± s.e.m. $^*P < 0.05$, $^{**}P < 0.01$, $^{***}P < 0.001$, and $^{****}P < 0.0001$. Please also see Fig. S6

transcriptional and protein levels. The OX86 group exhibited significantly higher levels of *Ctla4* compared with the IgG1 control group (Fig. 5B). However, FCM analysis revealed no significant difference in CTLA-4 protein levels between the two groups (Fig. S6A).

The degradation assay revealed that OX86 significantly accelerated CTLA-4 degradation in activated $CD8^+$ T cells (Fig. 5C). To further explore the in vivo effect of OX86 on CTLA-4 expression and the antitumor activity of $CD8^+$ T cells, OX86 and IgG1 (control) were intraperitoneally injected into B16-OVA tumor-bearing mice with adoptively transferred OT-I cells (Fig. 5D). FCM analysis reported a decrease in CTLA-4 expression in tumor-infiltrating OT-I cells in the OX86 group (Fig. 5E). The OX86 group exhibited slower tumor growth and an increased proportion of tumor-infiltrating OT-I cells (Fig. 5F, G). OX86 treatment significantly augmented the expression of Ki67, GZMB, perforin, FasL, and IFN-γ in tumor-infiltrating OT-I cells. However, it decreased the expression of TCF-1, and there was no significant difference in TOX expression (Fig. 5H, Fig. S6F, G). Given that the decreased expression of CTLA-4 may lead to the overactivation of the immune system [45], we measured the body weight and performed pathological analysis on the heart, lungs, kidneys, and liver in mice, and found that OX86 increased inflammatory infiltrates in the lungs (Fig. S6D) and exerted a slight effect on the body weight of mice (Fig. S6C). In addition, we also found a decrease of Tregs in tumors with OX86 treatment (Fig. S6E), which may contribute to the antitumor effect of OX86. The antitumor efficacy of Th9 cells is dependent on the upregulated expression of TRAF6 [29]. Subsequently, whether the antitumor activity of OX86 is dependent on TRAF6 was investigated. WT $CD45.2^+$ OT-I cells or *Traf6*-tKO $CD45.2^+$ OT-I cells were adoptively transferred into B16-OVA tumor-bearing $CD45.1^+$ $Rag1^{-/-}$ mice, which were then treated with OX86 (Fig. 5I). *Traf6* deficiency in OT-I cells attenuated the antitumor activity of OX86 (Fig. 5I). To further evaluate the synergistic antitumor effect of OX86 with ICB, B16-OVA tumor-bearing mice were treated with OX86 in combination with anti-programmed cell death 1 ligand 1 (PD-L1) or anti-CTLA-4 blocking antibodies. Compared with the anti-CTLA-4 antibody, the anti-PD-L1 blocking antibody significantly enhanced the antitumor efficacy of OX86 (Fig. 5J, K), suggesting a synergistic antitumor effect between OX86 and PD-1 pathway blockade.

The correlation between the OX40-TRAF6 axis and clinical features in melanoma patients

Finally, we assessed the correlation between the OX40-TRAF6 axis and clinical features in patients with melanoma. By analyzing RNA-sequencing data in The Cancer Genome Atlas (TCGA) datasets, we revealed that *TNFRSF4* and *TNFSF4* (which encode OX40 and the OX40 ligand, respectively) mRNA levels were significantly increased in melanoma tissues compared with normal tissues (Fig. 6A). However, there were no significant changes in *TRAF6* mRNA expression between the tissues (Fig. 6A). As the OX40-OX40L pathway induces TRAF6 expression [24], the infiltration level of immune cells in tumor tissues was analyzed in *TNFSF4/TNFRSF4* high- and low-expression tumor tissues. The number of $CD8^+$ T cells was significantly increased in the *TNFRSF4* and *TNFSF4* high-expression groups (Fig. 6B and Fig. S7A). Furthermore, correlation analysis using Spearman's rank-order method comparing *TNFSF4/TNFRSF4* expression and the infiltration levels (ImmuneScore) of tumor immune cells revealed a positive correlation between *TNFSF4/TNFRSF4* expression and tumor $CD8^+$ T-cell infiltration levels (Fig. 6C and Fig. S7B). A significant correlation between *TRAF6* expression and *TNFSF4* expression was found by analyzing the TCGA patients with melanoma database (Fig. S7C). Patients with high *TNFSF4/TNFRSF4* expression had a significantly better prognosis than those with low *TNFSF4/TNFRSF4* expression in the TCGA cohort, but patients with high *LRBA* expression did not (Fig. 6D and Fig. S7D). Overall, these results proved the relevance of a regulatory link between the OX40-TRAF6 axis and $CD8^+$ T-cell functional potency in human cancer.

DISCUSSION

In this study, we identified TRAF6 as a key ubiquitin E3 ligase that regulates CTLA-4 expression and T-cell antitumor activity. Moreover, OX40 signaling regulates the expression of TRAF6 and CTLA-4, with the results highlighting the OX40-TRAF6-CTLA-4 axis as a potential therapeutic target for tumor immunotherapy (Fig. S8).

CTLA-4 is a crucial immune checkpoint for T-cell activation and contributes to tumor immune evasion and degradation through the autophagy-lysosome pathway [19, 33, 46]. Our previous study showed that MG132 accelerates the degradation of CTLA-4 [33]. Given that MG132 has also been identified as an autophagy inducer by inducing p62 phosphorylation [47], we infer that the promotion of CTLA-4 degradation by MG132 may due to the activation of autophagic flux. Similar to the previous in vitro study on PD-1 expression in T cells that decreased after 72 h of TCR-activation [48], we also observed a decrease in CTLA-4 MFI 72 h activation, which may be due to exhaustion of the anti-CD3/CD28 antibody in the cell medium. To elucidate the degradation mechanism of CTLA-4 in T cells, its ubiquitin modification was assessed. In line with the findings of a previous study [49], CTLA-4 was found to be modified by ubiquitylation in activated $CD8^+$ T cells. In this study, we demonstrated that TRAF6 induces CTLA-4 protein degradation via binding to CTLA-4 and modifying it through K63-linked ubiquitylation. Given that LRBA deficiency reduces CTLA-4 expression by blocking its trafficking to lysosomes [19, 50], the relationship between TRAF6 and LRBA in CTLA-4 regulation deserves further investigation. However, whether TRAF6 directly binds to CTLA-4 or other proteins that participate in CTLA-4 degradation requires further investigation.

Our findings indicate that *Traf6* deficiency results in an increased CTLA-4 protein levels in T cells, which is consistent with previous studies by Ni et al and Dewayani et al. [51, 52]. Moreover, by using *Traf6*-deficient mice and retroviral overexpression experiments, we have confirmed that TRAF6 mediates CTLA-4 degradation in a T-cell-intrinsic manner, which is dependent on the RING domain of TRAF6. However, the crosstalk between TRAF6 and FOXP3 involved in the regulation of CTLA-4 expression requires further investigation. Worth noting is that, Lee et al showed that TRAF6 plays a pivotal role in activating autophagy in cancer cells [53], suggesting that enhanced autophagic flux by TRAF6 in T cells may be an additional layer of mechanism in regulating CTLA-4 degradation, which needs further investigation. Other checkpoint receptors (such as PD-1 and LAG3), which were downregulated in the *Traf6* overexpression group, maybe a potential mechanism involved in the regulation of the OX40-TRAF6 axis in antitumor $CD8^+$ T-cell immunity. Previous researchers have reported that *Traf6* knockout suppresses antitumor activity and IFN-γ production in $CD4^+$ T cells [21, 29]. The current results indicate that TRAF6 is critical for the antitumor activity of $CD8^+$ T cells, as *Traf6* deficiency results in impaired effector functions and higher TCF-1 expression in T cells. Although we demonstrated that TRAF6 promotes T-cell-mediated antitumor activity by regulating CTLA-4 degradation, the CTLA-4 independent regulatory mechanism of TRAF6 on needs further investigation. Given that TCF-1 is a crucial transcription factor in progenitor-exhausted T cells, it is plausible that TRAF6 might regulate the progenitor state of exhausted cells. These results highlight that TRAF6 regulates CTLA-4 degradation in a T-cell-intrinsic manner and is critical for antitumor responses of T cells.

The tumor necrosis factor receptor OX40 (CD134) plays a proinflammatory role in antiviral immunity and autoimmunity by regulating $CD4^+$ T-cell differentiation [54, 55]. Xiao et al. reported that OX40 signaling promotes the expression of TRAF6 and favors the induction of Th9 cells [24]. By using OX86, an OX40 agonist,

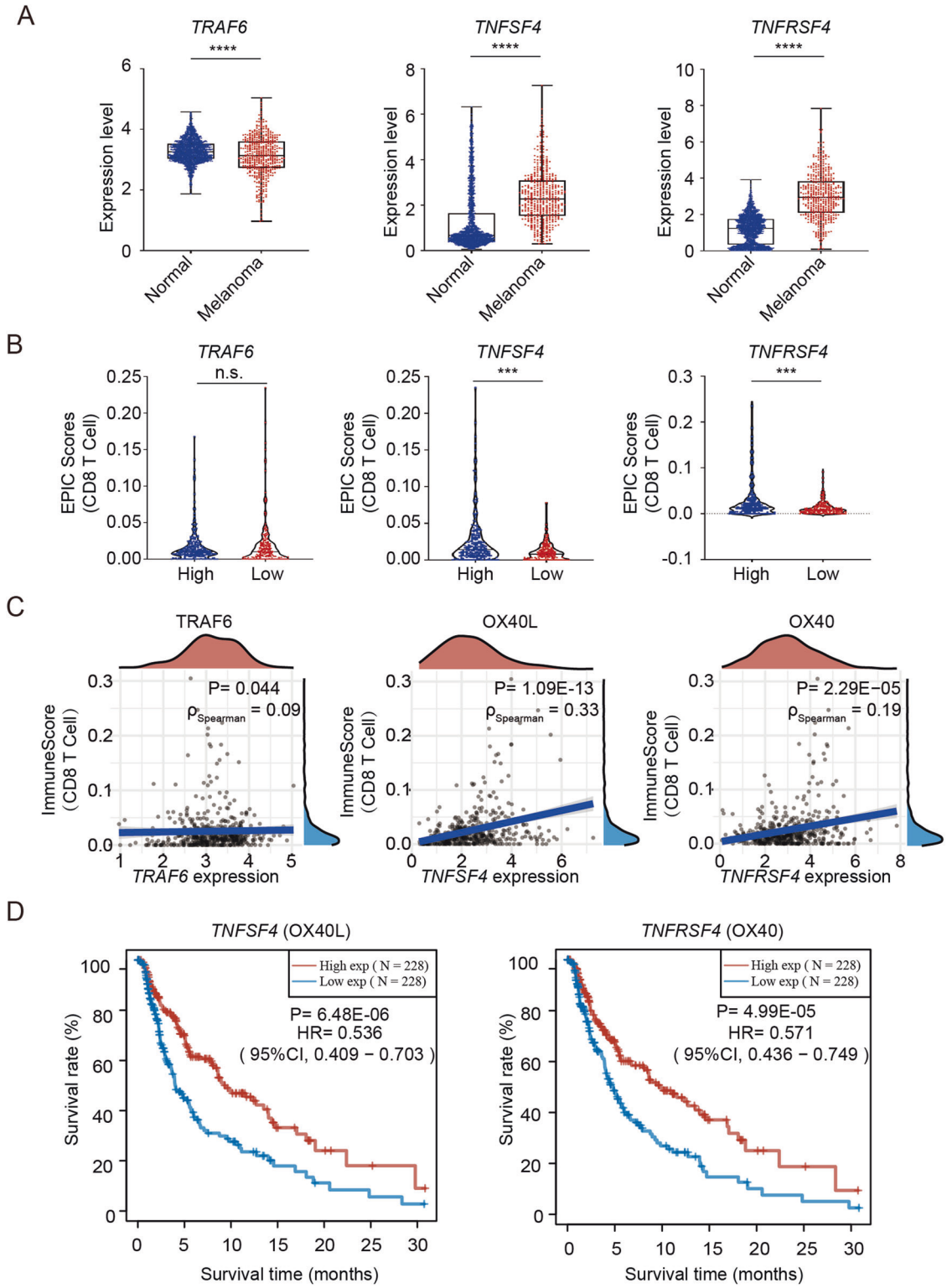

Fig. 6 The correlation between the OX40-TRAF6 axis and clinical features in melanoma patients. **A** The expression distribution of *TRAF6*, *TNFSF4* or *TNFRSF4* gene expression levels in melanoma and normal tissues. A two-sided Wilcox test. **B** The correlations between gene expression and ImmuneScore. The samples were grouped into high-expression (top 50%) and low-expression (bottom 50%) groups based on the average gene expression of *TRAF6*, *TNFSF4* or *TNFRSF4*. Spearman's rank-order correlation. **C** The correlations between gene expression of *TRAF6*, *TNFSF4* or *TNFRSF4* and ImmuneScore of $CD8^+$ T cells. **D** KM survival analysis of the gene signature from TCGA dataset. The samples were grouped into high-expression (top 50%) and low-expression (bottom 50%) groups based on the average gene expression of *TNFSF4* or *TNFRSF4*. KM survival analysis with the log-rank test was used. Error bars represent SD. EPIC Estimating the Proportions of Immune and Cancer Cells. $^*P < 0.05$, $^{**}P < 0.01$, $^{***}P < 0.001$, and $^{****}P < 0.0001$. $\rho_{Spearman}$, correlation coefficient. Please also see Fig. S7

in vitro and in vivo, OX40 signaling was shown to activate TRAF6 and facilitate CTLA-4 degradation and antitumor activity in $CD8^+$ T cells. Furthermore, the enhancement of antitumor T-cell responses by OX40 stimulation was TRAF6 dependent. A significant body of data suggests that the combination of PD-1 blockade and OX40 agonist strengthens the activation of $CD4^+$ and $CD8^+$ T cells during antitumor [56], antiviral [57], and anti-infection immunity [58]. In this study, an OX40 agonist was observed to coordinate with PD-1 but not CTLA-4 blockade in antitumor immunity. These results indicated that there are overlapping mechanisms between OX40 activation and CTLA-4 blockade in tumor immunotherapy. Given the different effects of OX40 activation and CTLA-4 blockade in immune cells, such as invariant natural killer T cells and neutrophils [59, 60], additional clinical investigations in cancer treatment are needed. In patients with melanoma, RNA-sequencing analysis revealed a positive correlation between the OX40 pathway and tumor-infiltrating $CD8^+$ T cells. Furthermore, OX40 signaling was associated with increased overall survival in patients with melanoma. By interrogating the TCGA database (data not shown), we found that there was no significant difference in *TRAF6* expression between melanoma tissues and normal tissues, and the expression of *TRAF6* had no correlation with $CD8^+$ T-cell infiltration in tumors and patient survival. Due to *TRAF6* is expressed primarily in myeloid cells [61–63], bulk RNA-seq of the tumor sample cannot reflect the expression of *TRAF6* in $CD8^+$ TILs. As gene expression in TILs cannot be analyzed by the TCGA database, further clinical studies are needed to strengthen our conclusions. Overall, our findings highlight the potential of the OX40-TRAF6-CTLA-4 axis as a viable therapeutic target for improving T-cell-based immunotherapies.

DATA AVAILABILITY

The GEO accession number for the RNA-sequencing data is GSE222539. MS data (PRIDE: PXD039327) have been deposited into the PRIDE Archive. All data needed to evaluate the conclusions made in this paper are presented in the paper or in Supplementary Materials. Additional data are available from the authors upon request.

REFERENCES

1. Carlino MS, Larkin J, Long GV. Immune checkpoint inhibitors in melanoma. Lancet. 2021;398:1002–14.
2. Walker LS, Sansom DM. The emerging role of CTLA4 as a cell-extrinsic regulator of T cell responses. Nat Rev Immunol. 2011;11:852–63.
3. Rowshanravan B, Halliday N, Sansom DM. CTLA-4: a moving target in immunotherapy. Blood. 2018;131:58–67.
4. O'Day SJ, Hamid O, Urba WJ. Targeting cytotoxic T-lymphocyte antigen-4 (CTLA-4): a novel strategy for the treatment of melanoma and other malignancies. Cancer. 2007;110:2614–27.
5. Brunner MC, Chambers CA, Chan FK, Hanke J, Winoto A, Allison JP. CTLA-4-Mediated inhibition of early events of T cell proliferation. J Immunol. 1999;162:5813–20.
6. Leach DR, Krummel MF, Allison JP. Enhancement of antitumor immunity by CTLA-4 blockade. Science. 1996;271:1734–6.
7. Schadendorf D, Hodi FS, Robert C, Weber JS, Margolin K, Hamid O, et al. Pooled analysis of long-term survival data from phase II and phase III trials of ipilimumab in unresectable or metastatic melanoma. J Clin Oncol. 2015;33:1889–94.
8. Takahashi A, Namikawa K, Ogata D, Nakano E, Jinnai S, Nakama K, et al. Real-world efficacy and safety data of nivolumab and ipilimumab combination therapy in Japanese patients with advanced melanoma. J Dermatol. 2020;47:1267–75.
9. Feng Y, Roy A, Masson E, Chen TT, Humphrey R, Weber JS. Exposure-response relationships of the efficacy and safety of ipilimumab in patients with advanced melanoma. Clin Cancer Res. 2013;19:3977–86.
10. Antonia S, Goldberg SB, Balmanoukian A, Chaft JE, Sanborn RE, Gupta A, et al. Safety and antitumour activity of durvalumab plus tremelimumab in non-small cell lung cancer: a multicentre, phase 1b study. Lancet Oncol. 2016;17:299–308.
11. Klocke K, Sakaguchi S, Holmdahl R, Wing K. Induction of autoimmune disease by deletion of CTLA-4 in mice in adulthood. Proc Natl Acad Sci USA. 2016;113:E2383–92.
12. Schubert D, Bode C, Kenefeck R, Hou TZ, Wing JB, Kennedy A, et al. Autosomal dominant immune dysregulation syndrome in humans with CTLA4 mutations. Nat Med. 2014;20:1410–6.
13. Kurtz J, Raval F, Vallot C, Der J, Sykes M. CTLA-4 on alloreactive CD4 T cells interacts with recipient CD80/86 to promote tolerance. Blood. 2009;113:3475–84.
14. Zhao Y, Chen S, Lan P, Wu C, Dou Y, Xiao X, et al. Macrophage subpopulations and their impact on chronic allograft rejection versus graft acceptance in a mouse heart transplant model. Am J Transpl. 2018;18:604–16.
15. Vincenti F, Rostaing L, Grinyo J, Rice K, Steinberg S, Gaite L, et al. Belatacept and long-term outcomes in kidney transplantation. N Engl J Med. 2016;374:333–43.
16. Kerdiles YM, Stone EL, Beisner DR, McGargill MA, Ch'en IL, Stockmann C, et al. Foxo transcription factors control regulatory T cell development and function. Immunity. 2010;33:890–904.
17. Gibson HM, Hedgcock CJ, Aufiero BM, Wilson AJ, Hafner MS, Tsokos GC, et al. Induction of the CTLA-4 gene in human lymphocytes is dependent on NFAT binding the proximal promoter. J Immunol. 2007;179:3831–40.
18. Chen C, Rowell EA, Thomas RM, Hancock WW, Wells AD. Transcriptional regulation by Foxp3 is associated with direct promoter occupancy and modulation of histone acetylation. J Biol Chem. 2006;281:36828–34.
19. Lo B, Zhang K, Lu W, Zheng L, Zhang Q, Kanellopoulou C, et al. AUTOIMMUNE DISEASE. Patients with LRBA deficiency show CTLA4 loss and immune dysregulation responsive to abatacept therapy. Science. 2015;349:436–40.
20. Walsh MC, Lee J, Choi Y. Tumor necrosis factor receptor- associated factor 6 (TRAF6) regulation of development, function, and homeostasis of the immune system. Immunol Rev. 2015;266:72–92.
21. Pearce EL, Walsh MC, Cejas PJ, Harms GM, Shen H, Wang LS, et al. Enhancing CD8 T-cell memory by modulating fatty acid metabolism. Nature. 2009;460:103–7.
22. Cejas PJ, Walsh MC, Pearce EL, Han D, Harms GM, Artis D, et al. TRAF6 inhibits Th17 differentiation and TGF-beta-mediated suppression of IL-2. Blood. 2010;115:4750–7.
23. Wilcox RA. A three-signal model of T-cell lymphoma pathogenesis. Am J Hematol. 2016;91:113–22.
24. Xiao X, Balasubramanian S, Liu W, Chu X, Wang H, Taparowsky EJ, et al. OX40 signaling favors the induction of T(H)9 cells and airway inflammation. Nat Immunol. 2012;13:981–90.
25. Bidère N, Snow AL, Sakai K, Zheng L, Lenardo MJ. Caspase-8 regulation by direct interaction with TRAF6 in T cell receptor-induced NF-kappaB activation. Curr Biol. 2006;16:1666–71.
26. Deng T, Hu B, Wang X, Ding S, Lin L, Yan Y, et al. TRAF6 autophagic degradation by avibirnavirus VP3 inhibits antiviral innate immunity via blocking NFKB/NF-kappaB activation. Autophagy. 2022;18:2781–98.
27. King CG, Kobayashi T, Cejas PJ, Kim T, Yoon K, Kim GK, et al. TRAF6 is a T cell-intrinsic negative regulator required for the maintenance of immune homeostasis. Nat Med. 2006;12:1088–92.
28. Xiao X, Fan Y, Li J, Zhang X, Lou X, Dou Y, et al. Guidance of super-enhancers in regulation of IL-9 induction and airway inflammation. J Exp Med. 2018;215:559–74.
29. Lu Y, Wang Q, Xue G, Bi E, Ma X, Wang A, et al. Th9 cells represent a unique subset of CD4(+) T cells endowed with the ability to eradicate advanced tumors. Cancer Cell. 2018;33:1048–60.
30. Zhang Q, Huang H, Zhang L, Wu R, Chung CI, Zhang SQ, et al. Visualizing dynamics of cell signaling in vivo with a phase separation-based kinase reporter. Mol Cell. 2018;69:334–46.
31. Chang D, Xing Q, Su Y, Zhao X, Xu W, Wang X, et al. The conserved non-coding sequences CNS6 and CNS9 control cytokine-induced Rorc transcription during T helper 17 cell differentiation. Immunity. 2020;53:614–26.
32. Wu J, Zhang H, Shi X, Xiao X, Fan Y, Minze LJ, et al. Ablation of transcription factor IRF4 promotes transplant acceptance by driving allogenic CD4(+) T cell dysfunction. Immunity. 2017;47:1114–28.e6.
33. Cui J, Yu J, Xu H, Zou Y, Zhang H, Chen S, et al. Autophagy-lysosome inhibitor chloroquine prevents CTLA-4 degradation of T cells and attenuates acute rejection in murine skin and heart transplantation. Theranostics. 2020;10:8051–60.
34. Zhang Y, Du X, Liu M, Tang F, Zhang P, Ai C, et al. Hijacking antibody-induced CTLA-4 lysosomal degradation for safer and more effective cancer immunotherapy. Cell Res. 2019;29:609–27.
35. Choi YB, Harhaj EW. HTLV-1 tax stabilizes MCL-1 via TRAF6-dependent K63-linked polyubiquitination to promote cell survival and transformation. PLoS Pathog. 2014;10:e1004458.
36. Strickson S, Emmerich CH, Goh ETH, Zhang J, Kelsall IR, Macartney T, et al. Roles of the TRAF6 and Pellino E3 ligases in MyD88 and RANKL signaling. Proc Natl Acad Sci USA. 2017;114:E3481–E9.
37. Ohtake F, Saeki Y, Ishido S, Kanno J, Tanaka K. The K48-K63 branched ubiquitin chain regulates NF-kappaB signaling. Mol Cell. 2016;64:251–66.
38. Cohen JL, Trenado A, Vasey D, Klatzmann D, Salomon BL. CD4(+)CD25(+) immunoregulatory T Cells: new therapeutics for graft-versus-host disease. J Exp Med. 2002;196:401–6.
39. Naito A, Azuma S, Tanaka S, Miyazaki T, Takaki S, Takatsu K, et al. Severe osteopetrosis, defective interleukin-1 signalling and lymph node organogenesis in TRAF6-deficient mice. Genes Cells. 1999;4:353–62.

40. Iwata A, Durai V, Tussiwand R, Briseno CG, Wu X, Grajales-Reyes GE, et al. Quality of TCR signaling determined by differential affinities of enhancers for the composite BATF-IRF4 transcription factor complex. Nat Immunol. 2017;18:563–72.
41. Danilo M, Chennupati V, Silva JG, Siegert S, Held W. Suppression of Tcf1 by inflammatory cytokines facilitates effector CD8 T cell differentiation. Cell Rep. 2018;22:2107–17.
42. Stickel N, Prinz G, Pfeifer D, Hasselblatt P, Schmitt-Graeff A, Follo M, et al. MiR-146a regulates the TRAF6/TNF-axis in donor T cells during GVHD. Blood. 2014;124:2586–95.
43. de Almeida PE, Mak J, Hernandez G, Jesudason R, Herault A, Javinal V, et al. Anti-VEGF treatment enhances CD8(+) T-cell antitumor activity by amplifying hypoxia. Cancer Immunol Res. 2020;8:806–18.
44. Jahan N, Talat H, Curry WT. Agonist OX40 immunotherapy improves survival in glioma-bearing mice and is complementary with vaccination with irradiated GM-CSF-expressing tumor cells. Neuro Oncol. 2018;20:44–54.
45. Beck KE, Blansfield JA, Tran KQ, Feldman AL, Hughes MS, Royal RE, et al. Enterocolitis in patients with cancer after antibody blockade of cytotoxic T-lymphocyte-associated antigen 4. J Clin Oncol. 2006;24:2283–9.
46. Boutros C, Tarhini A, Routier E, Lambotte O, Ladurie FL, Carbonnel F, et al. Safety profiles of anti-CTLA-4 and anti-PD-1 antibodies alone and in combination. Nat Rev Clin Oncol. 2016;13:473–86.
47. You Z, Jiang WX, Qin LY, Gong Z, Wan W, Li J, et al. Requirement for p62 acetylation in the aggregation of ubiquitylated proteins under nutrient stress. Nat Commun. 2019;10:5792.
48. Meng X, Liu X, Guo X, Jiang S, Chen T, Hu Z, et al. FBXO38 mediates PD-1 ubiquitination and regulates anti-tumour immunity of T cells. Nature. 2018;564:130–5.
49. Kennedy A, Waters E, Rowshanravan B, Hinze C, Williams C, Janman D, et al. Differences in CD80 and CD86 transendocytosis reveal CD86 as a key target for CTLA-4 immune regulation. Nat Immunol. 2022;23:1365–78.
50. Janman D, Hinze C, Kennedy A, Halliday N, Waters E, Williams C, et al. Regulation of CTLA-4 recycling by LRBA and Rab11. Immunology. 2021;164:106–19.
51. Ni X, Kou W, Gu J, Wei P, Wu X, Peng H, et al. TRAF6 directs FOXP3 localization and facilitates regulatory T-cell function through K63-linked ubiquitination. EMBO J. 2019;38.
52. Dewayani A, Kamiyama N, Sachi N, Ozaka S, Saechue B, Ariki S, et al. TRAF6 signaling pathway in T cells regulates anti-tumor immunity through the activation of tumor specific Th9 cells and CTLs. Biochem Biophys Res Commun. 2022;613:26–33.
53. Min Y, Kim MJ, Lee S, Chun E, Lee KY. Inhibition of TRAF6 ubiquitin-ligase activity by PRDX1 leads to inhibition of NFKB activation and autophagy activation. Autophagy. 2018;14:1347–58.
54. Jhajj HS, Lwo TS, Yao EL, Tessier PM. Unlocking the potential of agonist antibodies for treating cancer using antibody engineering. Trends Mol Med. 2023;29:48–60.
55. Kraehenbuehl L, Weng CH, Eghbali S, Wolchok JD, Merghoub T. Enhancing immunotherapy in cancer by targeting emerging immunomodulatory pathways. Nat Rev Clin Oncol. 2022;19:37–50.
56. Ma Y, Li J, Wang H, Chiu Y, Kingsley CV, Fry D, et al. Combination of PD-1 inhibitor and OX40 agonist induces tumor rejection and immune memory in mouse models of pancreatic cancer. Gastroenterology. 2020;159:306–19.e12.
57. Jacobi FJ, Wild K, Smits M, Zoldan K, Csernalabics B, Flecken T, et al. OX40 stimulation and PD-L1 blockade synergistically augment HBV-specific CD4 T cells in patients with HBeAg-negative infection. J Hepatol. 2019;70:1103–13.
58. Zander RA, Obeng-Adjei N, Guthmiller JJ, Kulu DI, Li J, Ongoiba A, et al. PD-1 Co-inhibitory and OX40 Co-stimulatory crosstalk regulates helper T cell differentiation and anti-plasmodium humoral immunity. Cell Host Microbe. 2015;17:628–41.
59. Jin H, Zhang C, Sun C, Zhao X, Tian D, Shi W, et al. OX40 expression in neutrophils promotes hepatic ischemia/reperfusion injury. JCI Insight. 2019;4.
60. Nuebling T, Schumacher CE, Hofmann M, Hagelstein I, Schmiedel BJ, Maurer S, et al. The immune checkpoint modulator OX40 and its ligand OX40L in NK-cell immunosurveillance and acute myeloid leukemia. Cancer Immunol Res. 2018;6:209–21.
61. West AP, Brodsky IE, Rahner C, Woo DK, Erdjument-Bromage H, Tempst P, et al. TLR signalling augments macrophage bactericidal activity through mitochondrial ROS. Nature. 2011;472:476–80.
62. Xu W, Dong J, Zheng Y, Zhou J, Yuan Y, Ta HM, et al. Immune-checkpoint protein VISTA regulates antitumor immunity by controlling myeloid cell-mediated inflammation and immunosuppression. Cancer Immunol Res. 2019;7:1497–510.
63. Tirosh I, Izar B, Prakadan SM, Wadsworth MH 2nd, Treacy D, Trombetta JJ, et al. Dissecting the multicellular ecosystem of metastatic melanoma by single-cell RNA-seq. Science. 2016;352:189–96.

ACKNOWLEDGEMENTS

The authors wish to thank Dr. Ding Ma (Huazhong University of Science and Technology) for providing the B16 and MC38 cells, Dr. Peng Zhang (Wuhan University) for the *Traf6*^{fl} mice, Dr. Xiangliang Yang (Huazhong University of Science and Technology) for the B16-OVA cells, Dr. Xiaokun Shu (University of California) for the SPARK system, Dr. Long Yu and Dr. Ning Li for their technical guidance, and Dr. Xiaoyi Li for the operational support. Furthermore, the authors acknowledge the Medical Subcenter at the HUST Analytical & Testing Center and the Center of Experimental Animals of Tongji Medical College for providing outstanding services. This study was supported by the National Natural Science Foundation of China (82071803, 82241217, and 82271811), Fundamental Research Funds for the Central Universities (2021GCRC037), and Project Funded by China Postdoctoral Science Foundation (2021M691155).

AUTHOR CONTRIBUTIONS

Designed the experiments: JX, JW, DZ; Performed the biological experiments: JY, JC, YL, YZ; Generated cell lines: YN. SW; Performed the bioinformatic analysis: WY, HX, ZC; Analyzed the biological data: SR, SW; Wrote the manuscript (original draft): JY, JC, CZ; Wrote the manuscript (review & editing): XZ, JW.

COMPETING INTERESTS

The authors declare no competing interests.

ADDITIONAL INFORMATION

Supplementary information The online version contains supplementary material available at https://doi.org/10.1038/s41423-023-01093-y.

Correspondence and requests for materials should be addressed to Jiahong Xia or Jie Wu.